Program Digest, 2019 IEEE International Ultrasonics Symposium (IUS)
Glasgow, Scotland, October 6-9, 2019

Transient response of BAW resonators

B. Ivira, C. Kirkendall
Wireless Semiconductor Division
Broadcom Inc.
San Jose, USA

Lauri Lipiainen
Wireless Semiconductor Division
Broadcom Inc.
Munich, Germany

***Abstract*—The high demand for die size reduction and higher power levels in front-end modules to accommodate growing complexity pushes bulk acoustic wave (BAW) devices further into the nonlinear regime. Therefore, in order to reduce or cancel them, it is important to determine how they manifest in film bulk acoustic resonator (FBAR). Lately, the idea that pulsing RF signals could be used to qualify FBAR filters while reducing the dissipated energy has been investigated, therefore the pulsed RF scheme enables the measurement of the electrical and thermal transient responses of BAW resonators with a special focus in the Duffing region. Nonlinear phenomena elicited within the thermal Duffing region are measured in both transient and steady state regime using thermal and acoustic imaging. In addition, a fully coupled 3D finite element model (FEM) of FBAR gives further insight into the observed transient dynamics.**

Keywords—BAW, FBAR, self-heating, transient, FEM, FEA, thermal, Duffing, hysteresis, multistability, pulsed RF, energy confinement, acoustic imaging.

I. INTRODUCTION

Over the past few years, the emerging market for high power user equipment (HPUE) and the yearly die size reduction target of 20%, has pushed the power density in filtering functions in front-end modules to a much a higher level. To ensure both the smallest die size and best performances on the market, we highlight the need for deep understanding of nonlinearities under power in bulk acoustic wave (BAW) technologies. While steady-state analysis based on RF measurements, circuit modeling and finite element modeling (FEM) [1-6] of BAW devices under high RF power has received much attention, the thermal and mechanical transient responses are still fairly unexplored. The dominant mechanism of heat transfer in BAW resonators is thermal conduction, which is a relatively slow diffusion mechanism that affects the electro-acoustic dynamics of FBAR in the sub-millisecond range. In terms of electro-thermal dynamics, the thermal time scale defines the range of RF pulse width and pulse period that can be applied for exploring the origin of the thermal transient mechanisms, which in turn determine the frequency response as energy builds up over time. The pulsed RF signal is synchronized to a high speed thermal imager to give a direct reading of temperature vs. time. The high speed camera provides the thermal response vs. time analogous to an oscilloscope for electrical signals. In the scope of this research work, a fully coupled 3D finite FEM of FBAR further elucidates how the thermo-piezoelectric fields evolve on route to steady state. In addition to the experimental transient study using pulsed RF, we also apply a continuous wave (CW) signal to FBAR samples near the Duffing region and study their electrical, thermal, and acoustic steady-state behavior. For characterizing the acoustics during thermal Duffing, a custom-made full-field interferometer [7] is used to measure the out-of-plane (vertical) surface vibration fields on FBAR samples. The measured acoustic displacement reveals the different modes that co-exist in the active area during a thermal Duffing event.

II. ELECTRICAL, THERMAL AND MECHANICAL TRANSIENT RESPONSES

A. Pulsed RF

Pulsed radio frequency (RF) measurements allow us to take snapshots of the resonator impedance at given moments during the thermal transient response as the device heats up under the stimulus of a high power (HP) tone. In this particular experiment, the S-parameters acquisition is nearly two orders of magnitude faster than the thermal time scale of FBAR away from f_s, so the electrical response is not averaged out over a large temperature variation but in a nearly constant temperature narrow window. In order to meaningfully measure hot S-parameters [8] during very short bursts of RF power, one must understand the dynamics of the signal in both frequency and time domain. Standard S-parameters rely on the ratio of a and b waves under CW condition but pulsing that signal is in theory equivalent to windowing the RF sinusoidal wave by a rectangular pulse of period Te. Let's assume a CW signal g defined by (1) and the rectangular function Γ with a pulse width τ defined by (2).

$$g(t) = A\cos(2\pi f_0 t) \tag{1}$$

$$\Gamma(t) = \begin{cases} 1 \; if \; t \in [0, \tau] \\ 0 \; if \; t \in [\tau, Te] \end{cases} \tag{2}$$

The two signals g and Γ are multiplied in the time domain, resulting in a pulsed cosine. Experimentally, a pulse modulator modulates the RF source by the rectangular signal with an adjustable pulse width and period. The spectral response of each signal is given by its Fourier transform (3).

$$F\,(f) = \int_{-\infty}^{\infty} f(t) e^{-i2\pi ft} dt \tag{3}$$

The Fourier transform (4) of the RF cosine signal produces two Dirac delta function at fo and $-fo$.

$$G\,(f) = \int_{-\infty}^{\infty} \frac{e^{i2\pi f_0 t} + e^{-i2\pi f_0 t}}{2} e^{-i2\pi ft} dt$$

$$= \frac{A}{2}[\delta(f - f_0) + \delta(f + f_0)] \tag{4}$$

The Fourier transform of the rectangle signal provides a sine cardinal (5) where the secondary lobes span is inversely proportional to τ, i.e.$1/\tau$, see Fig. 1.

$$\Gamma\,(f) = \int_0^{\tau} e^{-i2\pi ft}\, dt$$
$$= \tau\ sinc(\pi f\tau) \quad (5)$$

The frequency response of the windowed cosine is the convolution of the RF cosine with the rectangular signal given in (6) and (7).

$$F\,[g(t).\Gamma(t)] = G\,(f) * \Gamma\,(f) = \int_{-\infty}^{\infty} G\,(f_G)\Gamma\,(f - f_G)\, df_G \quad (6)$$

$$G\,(f) * \Gamma\,(f) = \frac{A\tau}{2}[sinc(\pi\tau(f - f_0)) + sinc(\pi\tau(f + f_0))] \quad (7)$$

$$PSD = \int_{-\infty}^{\infty} |f(t)|^2 dt = \int_{-\infty}^{\infty} |F(f)|^2 df \quad (8)$$

Parseval's theorem in (8) states that the total power of a function is the same in the time domain and frequency domain. Consequently, as the pulse width of the pulsed signal gets narrower, the power spreads out in the spectrum, in other words the power spectral density (PSD) decreases.

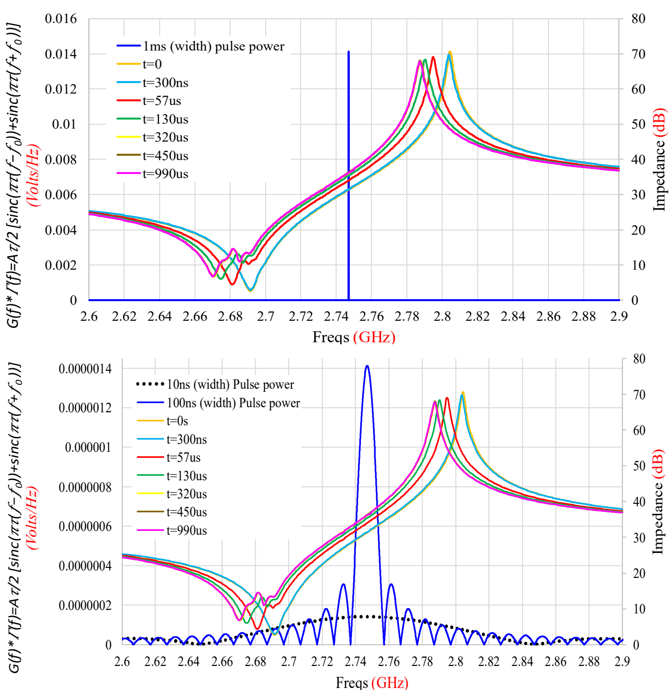

Fig. 1. Example of spectral response of the FBAR impedance captured at different times during a 1ms pulse width (*Pincident=a.u.*; *fo*=2747MHz), superimposed on the calculated sine cardinal for a 1ms, 100ns and 10ns pulse width and centered near the max group delay (2747MHz) of the resonator. The voltage $A = \sqrt{8.Pincident.Zo}$ with *Zo*=50Ohms.

Superimposing the sine cardinal stimulus and the impedance of the resonator as depicted in Fig. 1 shows that pulse widths on the order of 10-1000µs spread the energy over an approximately constant (or slow varying) region of the electrical response of the FBAR, and thus is still fairly comparable to a CW signal in term of frequency span. However, pulse widths in the 10-100ns range or lower would certainly reduce the peak temperature in the resonator but also spread out the energy over largely varying regions of power dissipation, especially when the RF pulse is applied near f_s. In a real application, pulsing an RF signal of a given period with an excessively narrow pulse (~1-10ns) would dramatically reduce the power in a given channel during transmission, and the energy could undesirably leak into the neighboring channels depending on the application. At 100ns pulse width, the main lobe has a width of $2/\tau$, similar to a 20MHz long term evolution (LTE) signal. Experimentally, the authors were interested in evaluating the thermal transient response of FBAR and how it affects the electrical response. As such, one of the experiments consisted in applying a 1ms pulse width high power signal at Pincident=*a.u.* (abritrary unit) around the max group delay (~2747MHz) of the resonator. The *a* and *b* waves were captured in a very short time (hundred nanoseconds or less to a few microseconds depending on the settings of the receiver) at different times (t=0s, 300ns, 57µs, 130µs, 320µs, 450µs, 990µs) during a given pulse width such that S-parameters can be reconstructed over the pulse train as the heat spreads across the resonator on its way to steady-state.

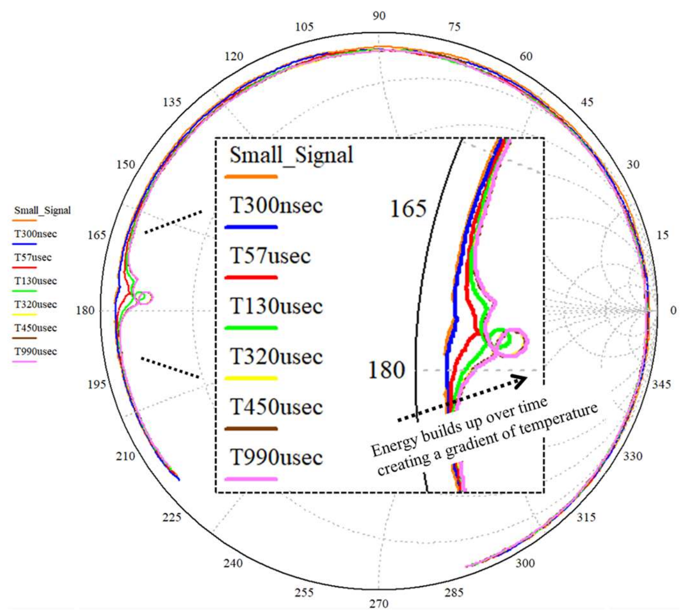

Fig. 2. FBAR impedance captured at different times during a 1ms pulse width using pulsed Hot S-parameters (same measurement in Fig. 1)

At t=0, defined as the small signal condition just before the HP tone hits the resonator, the series resonance is clearly defined as an impedance minima because the temperature of the membrane is near room temperature and uniform over the active area, as depicted in Fig. 1. At t=300ns, the pulsed HP tone has stressed the FBAR for nearly 300ns, but the dissipated energy hasn't had time to diffuse across the membrane. From t=300ns to t=320µs, the temperature gradient builds up across the active area and alters the electroacoustic response by locally modulating the stiffness and loss of each material. Above t=320µs, the resonator has reached steady state temperature for this particular stress stimulus away from f_s, as shown by the overlapping responses at t=320µs, t=450µs and t=990µs (Fig.2). During the transition, "self-heating loops" build up near f_s as measured by the pulsed hot S-parameters (Fig. 2), indicating that a temperature gradient exists across the resonator, as show in the steady state regime in Fig. 3, the temperature gradient is purposely exacerbated in this particular FBAR . If the thermal gradient due to the high power tone is large enough, then some portion of the cooler region will be below the local cutoff frequency of long wavelength lateral modes as the probe tone is swept near f_s. All hotter regions will lie above their local cutoff frequency. Thus, the hotter portion has a more uniform power dissipation profile, while the cooler region has a less uniform profile that tracks the long wavelength of the lateral modes, as explained in section III. For a given probe tone (small signal combined to the HP tone [8]) frequency, the boundary between the two is the isoline operating exactly at the lateral mode cutoff frequency, which partitions the resonator into two regions vibrating out of phase, as shown in section III. This distribution of "local f_s" due to the temperature gradient manifests as the additional modes in the Smith chart.

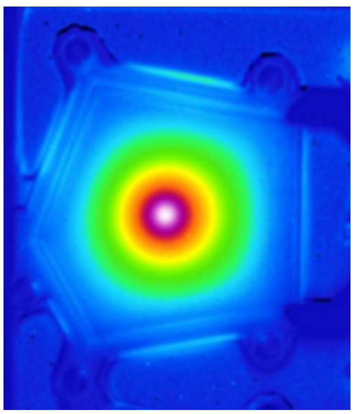

Fig. 3. Example of measured energy confinement (strong temperature gradient) in a thermal Duffing event where the resonator is purposely locked into self-heating (Tmax: 262.2C).

B. *Thermal transient*

Fig. 4 shows the thermal response at the center of the membrane (a higher frequency resonator than the one measured and presented in the previous II.*A*) during a 1ms RF pulse excitation. The transient response strongly depends on the driving frequency (scanned from below *fs* to *fp*) at constant incident power. The closer the driving tone is to the bifurcation frequency, the longer it takes for the resonator to reach steady state. This is related to the well-known bottlenecking phenomenon in which the resonator dynamics are slowed down during passage through the bifurcation. Although bottlenecking has been observed in the context of the mechanical Duffing effect as the driving frequency is swept through the bifurcation [9-10], here we report the first transient measurements of a thermal Duffing effect at fixed frequency near the bifurcation and show a slowing down effect during passage to steady state. Fig. 4 shows that in this case the transient bifurcation dynamics cause the temperature to deviate from the exponential response expected from a simple consideration of a thermal time constant determined by heat capacity and thermal conductivity of the FBAR. Away from the jump event associated with the sharp increase in power dissipation, the temperature in the active area reaches steady state in nearly the time of a LTE symbol period [11].

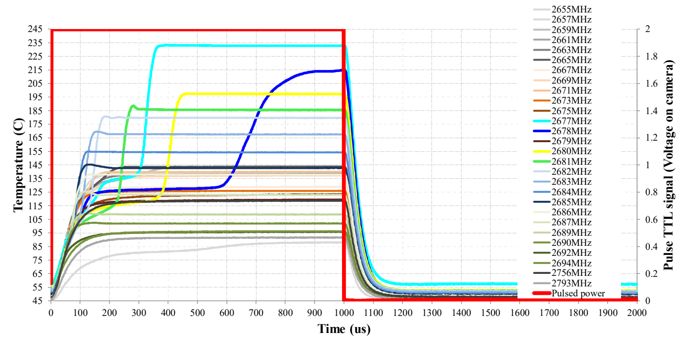

Fig. 4. Measured thermal response of FBAR for various stress stimulus from below *fs* to *fp*, at *Pincident=a.u.* (pulse width/period: 1ms/2ms), and 45C base temperature.

Yet, in the vicinity of the bifurcation point, the time it takes to reach steady state can be more than twice that when driving the device far away from the bifurcation frequency. Moreover, right at the bifurcation point, the resonator is very sensitive to initial conditions, as highlighted in Fig. 5. The traces t_1 to t_5 were recorded one after another over a 1-2s interval, and at the same driving power and frequency. Although the same repeated pulse is applied, slight changes in initial conditions result in large variations in the transient response as shown in Fig. 5.

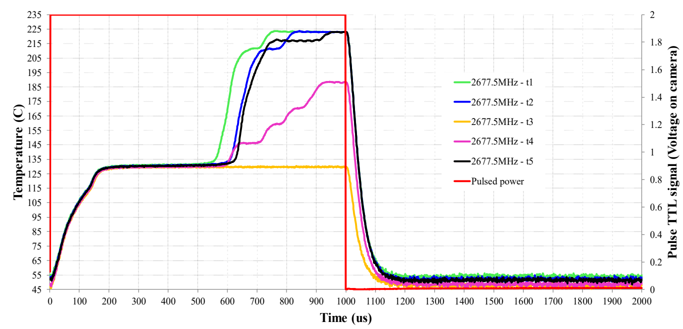

Fig. 5. Measured thermal response of FBAR captured at different times (t1, t2, t3, t4 and t5), for same stress stimulus near the bifurcation point, at *Pincident=a.u.* (pulse width/period: 1ms/2ms), and 45C base temperature.

A fully coupled 3D FEM model enables a closer look at how the displacement profile evolves with increasing thermal gradient. Fig. 6 shows a simulation of FBAR driven, in one case with a HP tone slightly below the saddle-node bifurcation frequency corresponding to the upwards jump, and another slightly above it. When the driving frequency is below the bifurcation point the wavelength of the TE1 modes increases as the resonator heats up over time. Since the resonator is not yet being driven beyond the bifurcation frequency, the entire active area remains below its local TE1 cutoff. On the other hand, for a HP tone frequency slightly above the bifurcation frequency but still below the cold f_s, the entire active area starts out below its local TE1 cutoff, but steadily develops a region in the center operating above the TE1 cutoff. From the simulated displacement profile this occurs as a distinct region out of phase with the cooler portion of the resonator that expands in size as the temperature increases. In terms of the power dissipation, as the thermal gradient increases over time during the transient phase, the power dissipation density becomes confined in the center of the resonator, but ultimately shifts to the edge of the resonator before reaching steady state [12].

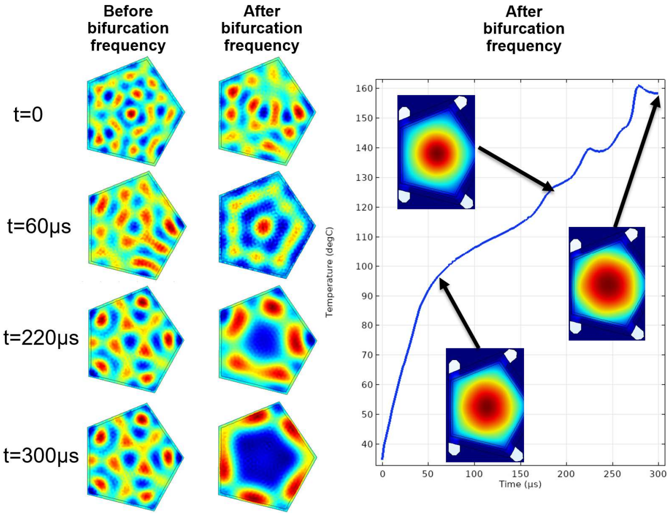

Fig. 6. Simulated displacement and temperature vs time near the bifurcation frequency. For a driving frequency less than the bifurcation frequency the entire active area is below the local TE1 cutoff. However, for driving frequencies greater than the bifurcation frequency but less than the "cold" f_s the center of the resonator transitions above its local TE1 cutoff during the transition to steady state. Of course, for driving frequencies above the "cold" f_s the entire active area starts out above its local TE1 cutoff (not shown in the figure above).

This energy confinement has the effect of increasing the effective thermal resistance referenced to a uniform heat source, because the heat must travel on average a longer distance to reach the thermal ground. In turn, during the phase of energy confinement the resonator experiences another sharp increase in temperature, which explains the double step shape of the temperature vs. time plot. In effect, the instantaneous time constant is changing as the effective thermal conductivity changes. This can be seen in the simulated temperature profiles of Fig. 6 as an increase or decrease in the thermal gradient over time. In other words, the hot spot becomes more or less concentrated in the center of the resonator depending on the distribution of power dissipation over the active area and the thermal resistance of the membrane.

C. Mechanical Transient

In the 3D FEM simulations above, the piezoelectric physics are simulated in the frequency domain and the time averaged power dissipation is used as a heat source in the heat transfer physics. To justify this approach, it is necessary that the timescale of acoustic dynamics be much shorter than that of the thermal dynamics. In other words, any large changes in temperature must occur over a timescale much longer than the mechanical time scale. To quantify this, a time-domain simulation of FBAR was carried out, as shown in Fig. 7. To simulate a worst case situation, the damping was chosen to be lower than typically occurs in FBAR. In this case the resonator still reaches steady state within 1 to 2μs. This means that technically, the temperature distribution within the first microsecond of simulation is not reliable. However, once the mechanical dynamics reach steady state, one can assume the acoustic dynamics adjust to their new steady state "instantaneously" due to relatively slow changes in temperature, justifying the hybrid frequency / time domain simulation approach.

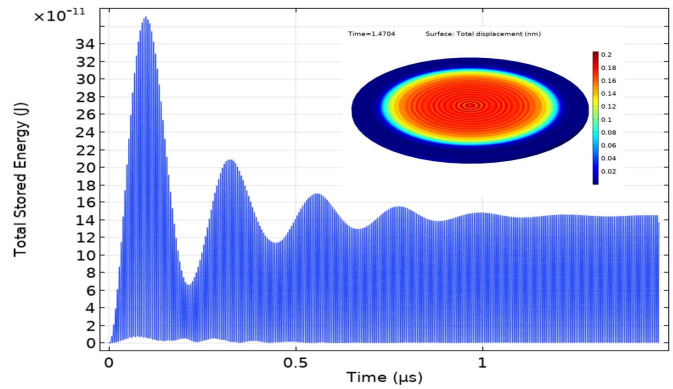

Fig. 7. Simulated mechanical response of FBAR during mechanical transient.

III. THERMAL DUFFING EFFECT

As described in [12-13], the thermal Duffing effect manifests most strongly at f_s in the form of hysteresis under specific and relatively high power and temperature conditions, and possibly in the rattle region of the resonator if rattles are poorly suppressed. Under steady-state conditions, the signature of the thermal Duffing effect is multistability, with the steady-state solution depending on initial conditions and the sweep direction of the driving frequency. Duffing behavior can be activated near any eigenfrequency of the resonator, but due to suppression of spurious modes using boundary frames, it is only pronounced at f_s and under sinusoidal wave excitation. Under LTE or 5G signals, the thermal Duffing effect hardly exists owing to the dynamic allocation in frequency and time of resource blocks in channels and modulation protocols in slots/subframes. During a downsweep with a CW signal, if the incident power remains on, the resonator can be locked into a solution branch with higher temperature than occurs during an upsweep, as shown in Fig. 8.

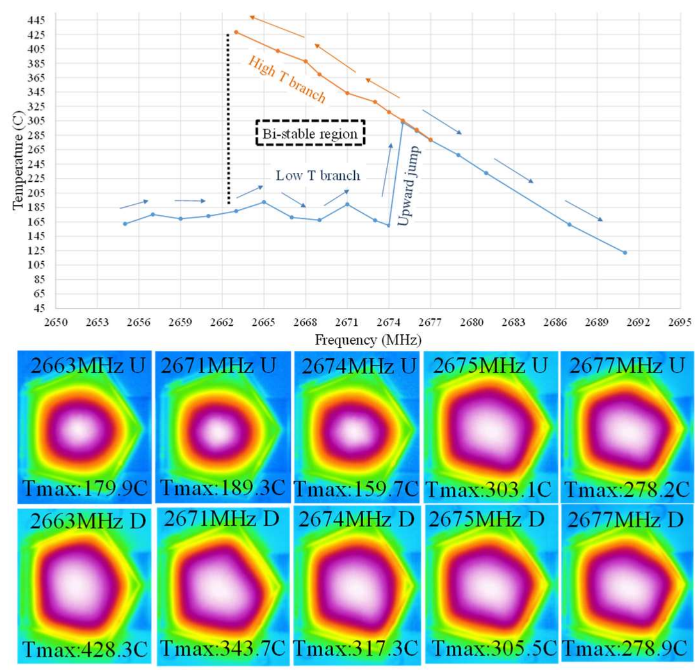

Fig. 8. Measured thermal Duffing effect in steady-state condition (U: up sweep /D: Down sweep), CW at constant incident power.

Turning off the power between frequency steps will always result in the resonator choosing the lower temperature branch. The sustainability in the high-T branch depends exclusively on the initial condition, which is related to the previous temperature condition every time the frequency is swept down. The origin of the effect resides in the fact that the electro-thermal response tracks the softening of the stiffness due to the negative temperature coefficient of stiffness while the temperature increases, and the resonator does not significantly cool down between steps as the driving frequency is decreased. The FBAR generally has a negative temperature coefficient of frequency, but a positive temperature coefficient of frequency of the resonator would revert the direction of the driving frequency needed to lock the resonator in the high-T branch. One has to note that the steady state temperature shown in Fig. 8 has slightly higher peak temperatures than in the thermal transient section. This is because the sensor of the high speed transient camera averages the temperature over a few thousand detectors while the sensor used for steady-state measurements does not. This is equivalent to a larger pixel size than the steady state camera, but still smaller than the active area of the resonator.

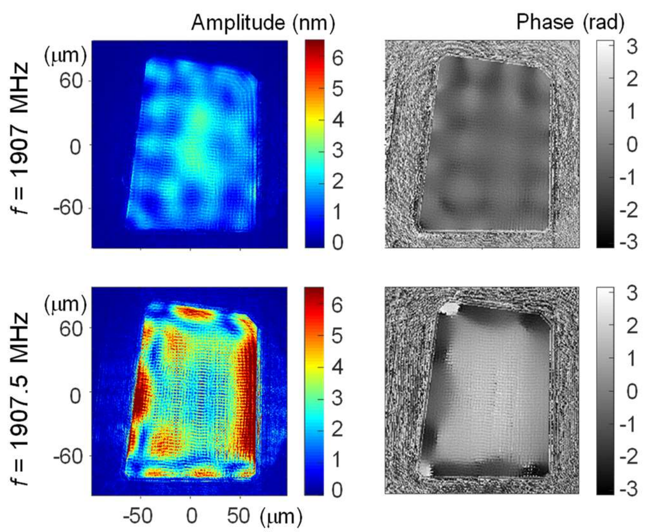

Fig. 9. Interferometric measurement of the amplitude and phase of the out-of-plane vibration field during thermal Duffing event at constant incident power (low-T branch on top and high-T branch at the bottom). In the high-T branch, the vibration amplitude is much larger than in the low-T branch, particularly at the edges.

Analogously to the temperature measurements in Fig. 8, full-field interferometry was applied to obtain the vibration amplitude in the frequency up- and down-sweeps. Fig. 9 shows the measured acoustic displacement of a different resonator (square shape and thickness) under steady state condition and confirms that the resonator vibrates below TE1 cutoff frequency in the low-T branch, and above TE1 cutoff frequency in the high-T branch, the thermal Duffing forces the center region of the resonator to vibrate more uniformly in a piston-like motion above TE1 cutoff. The amplitude data in Fig. 10 clearly shows the hysteresis effect due to thermal Duffing. During the up-sweep, the response jumps from the lower-T branch to the higher-T branch at 1908MHz. In the down-sweep, the response is locked to the higher-T solution branch and the downward jump occurs at much lower frequency (1900MHz) in that case. No such behavior is obtained at lower power as the resonator is operating in the linear regime. It should be noted that the out-of-plane amplitude pattern varies greatly as a function of frequency, resulting in large changes of the local amplitude values on the resonator surface. Here the amplitude values were averaged over a small region (see the inset in Fig. 10) and therefore the line plots do not look as smooth as the clear trend of temperature plots. Nevertheless, as can be seen from Fig. 9, the 2D amplitude and phase fields between the two states are dramatically different.

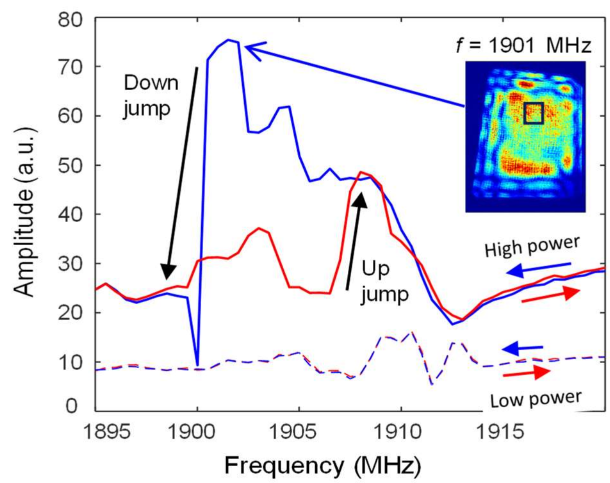

Fig. 10. Interferometric measurement of the out-of-plane amplitude during frequency up-sweep (red lines) and down-sweep (blue lines) at high power (solid lines) and much lower (dashed lines) incident power. The vibration amplitude field at f = 1901MHz of the frequency down-sweep at the higher power is shown on the top-right inset. The amplitude values for the line plots are calculated from the area illustrated in the inset with a black rectangle.

Differently from a CW signal, using an RF pulse excitation and depending on how long the RF pulse excitation remains off between RF bursts, the resonator may have time to cool down enough to prevent selection of a high-T solution branch, thus disabling any hysteresis in the spectrum below the bifurcation point. The electrical and thermal responses resulting from up and down sweeps could coincide, even with a sinusoidal excitation. If the durations of the on/off states of the RF pulses are short enough, the resonator would stay in the transient regime and would never reach steady-state.

IV. Conclusion

This work provides a detailed study about the limits of BAW technology in term of nonlinearities generated by thermal Duffing arising from extreme conditions of self-heating. Pulsing high power RF signals in the 10-1000ns range would greatly reduce the temperature in FBAR preventing this effect to take place but it also spreads the energy in the spectrum, and the mechanical time scale of FBAR under very narrow burst of high RF power would have to be accounted in the device response. Nevertheless, Broadcom Inc. inventions [14-16] allow to keep the resonator cool as needed to avoid severe nonlinear effect in BAW devices that are highlighted in the literature for the first time here from best author knowledge. Although severe conditions were applied to the resonators, none of them were destroyed by the power and temperature involved during those experiments.

References

[1] A. Tag A. R. Weigel, A. Hagelauer, B. Bader, C. Huck, P. Pitschi and D. Karolewski, "Influence of dissiapted power distribution on BAW resonators' behavior," in *Proc. IEEE Int. Ultrasonics Symp.*, Oct. 2014.

[2] M. Fattinger P. Stokes and G. Fattinger, "Thermal modeling of WLP-BAW filters: Power handling and miniaturization," in *Proc. IEEE Int. Ultrasonics Symp.*, Oct. 2015.

[3] C. Kirkendall and B. Ivira, "A Hybrid 3D Thermal / 1D Piezoelectric Finite Element Model for Rapid Simulation of FBAR Filter Response under High Power," in *Proc. IEEE Int. Ultrasonics Symp.*, Oct. 2018.

[4] B. Ivira, R-Y. Fillit, F. Ndagijimana, P. Benech, G. Parat and P. Ancey, "Self-heating Study of Bulk Acousic Wave Resonators Under High RF Power," in *IEEE Trans. On Ultrasonics, Ferroelectrics, and Frequency control*, Jan. 2008, vol. 55, no.1.

[5] S. Setoodeh, U. Kemiktarak, F. Bayatpur, S. Fouladi, and D. Feld, "A High Power Circuit Model of an FBAR Resonator for Use in Filter Design," in *Proc. IEEE Int. Ultrasonics Symp.*, Oct. 2019.

[6] Brice Ivira and Christopher Kirkendall, private communication, 2016.

[7] K. L. Telschow, V. A. Deason, D. Cottle, J. D. Larson III, "Full-Field Imaging of Gigahertz Film Bulk Acoustic Resonator Motion," in *IEEE Trans. On Ultrasonics, Ferroelectrics, and Frequency control*, Oct. 2003, vol. 50, no.10.

[8] B. Ivira, J. Larson, I. Ruby, T.Jamneala, C. Kirkendall, D. Figueredo, L. Kekoa and R. Ruby, "Integrated split 3-Bar resonator structure for higher power handling capability," in *Proc. IEEE Int. Ultrasonics Symp.*, Sep. 2016, pp. 1–6.

[9] Burgner, C. B., Turner, K. L., Miller, N. J., & Shaw, S. W., "Parameter sweep strategies for sensing using bifurcations in MEMS," *Solid-State Sensors, Actuators, and Microsystems Workshop* (2010).

[10] C. R. Kirkendall and J. W. Kwon. "Multistable internal resonance in electroelastic crystals with nonlinearly coupled modes," *Scientific Reports*, vol. 6, p. 22897, 2016.

[11] M. Rumney, "LTE and the evolution to 4G wireless," *Book*, *Wiley & Sons.*, 2013.

[12] C. Kirkendall and B. Ivira, "A fast thermo-piezoelectric finite element model of 3D transient FBAR dynamics under large RF signal," in *Proc. IEEE Int. Ultrasonics Symp.*, Oct. 2018.

[13] Brice Ivira, analytical circuit model and measurement of the thermal Duffing and multistability in FBAR, June 2014, Broadcom Inc. internal documents.

[14] Patent "10,284,168".

[15] Patent "10,177,736".

[16] Patent "16/521,640".